Lab on a Chip

Accepted Manuscript

ROYAL SOCIETY OF CHEMISTRY

www.rsc.org/loc

A simple microfluidic dispenser for single-microparticle and cell samples.

A. Kasukurti[1], C.D. Eggleton[2], S.A.Desai[3], D. I. Disharoon[1], D.W.M. Marr[1]

[1]Chemical and Biological Engineering, Colorado School of Mines, [2]Department of Mechanical Engineering, University of Maryland, Baltimore County, [3]Laboratory for Malaria and Vector Research, National Institute of Allergy and Infectious Disease, Bethesda, MD

Non-destructive isolation of single-cells has become an important need for many biology research laboratories; however, there is a lack of easily employed and inexpensive tools. Here, we present a single-particle sample delivery approach fabricated from simple, economical components that may address this need. In this, we employ unique flow and timing strategies to bridge the significant force and length scale differences inherent in transitioning from single particle isolation to delivery. Demonstrating this approach, we use an optical trap to isolate individual microparticles and red blood cells that are dispensed within separate 50 µl droplets off a microfluidic chip for collection into microscope slides or microtiter plates.

1. Introduction:

Single cell isolation techniques have helped push the frontiers of microbiology by making possible studies of the physiology and molecular biology of individual cells[1], the screening for novel enzymes and antibiotics[2] and the purification and cultivation of rare microbes[3]. Enabling these studies, techniques such as dilution-to-extinction[4], micromanipulation[5], flow cytometry[5], microfluidics[6-8] and compartmentalization[9] have been developed; however most of these techniques have proven tedious or time consuming because of the extensive manipulation required. Overcoming some of these limitations, microfluidics have shown promise because of the predictable flow profiles, fast switching times, and small reagent volumes. With the potential for a precise, high throughput, inexpensive and easy to use technique, technologies including dielectrophoretic assisted cell sorting (DACS) [7,10-12], micro-fluorescence-activated cell sorting (µFACS)[7,13-15], magnetic-activated cell sorting (MACS)[8,16,17] and optical trapping[18-21] using light scattering and gradient forces have been developed for cell detection and sorting within microfluidic platforms. While these approaches can be effective, they are designed to deliver cells to other on-chip compartments for collection or other analysis. In this, there is no clear approach for removal of generated samples from the micro- to the macro-world without compromising the sample and risking contamination. This has led to significant effort in the development of microfluidic platforms that incorporate post-processing assays such as PCR[22], western blotting[23] and protein microarrays[24] increasing cost and complexity[25]. While such fully functional devices have important applications, additional hardware is counter to the goal of microfluidics and there remains a need for simple systems that can interface well with available and extremely capable laboratory instrumentation.

While cell sorting throughput can be a significant drive for many applications and commercial tools such as BDCloneCyt available within core facilities, they can be expensive and not appropriate for individual researcher labs. As a result, there is a need for a simple and flexible technology that can accurately dispense single cells off chip to achieve the low throughputs required for 96 well plates. We report here the development of a microfluidic technology that continuously dispenses isolated single microparticles through encapsulation into 50 µl droplets for deposition onto any substrate. We demonstrate function with red blood cells (RBCs) isolated with a bench-top optical trap onto microscope slides. We also demonstrate an inexpensive and compact implementation of the same with 4.18 µm fluorescent polystyrene microparticles isolated with an off-the-shelf DVD optical pickup generated optical trap[26]. With no need for external pumps or active components this is an inexpensive and easy to operate system. This device could serve as a portable and inexpensive alternative to limiting dilution techniques while achieving accuracies close to flow cytometers for supplying non adherent single cell samples at throughputs necessary for smaller research laboratories needing cultivation of homogenous cell populations for genetics, pharmacology and pathology. The entire setup can be automated and made compact enough to fit in a sterile environment such as a cell culture hood.

2. Materials and methods

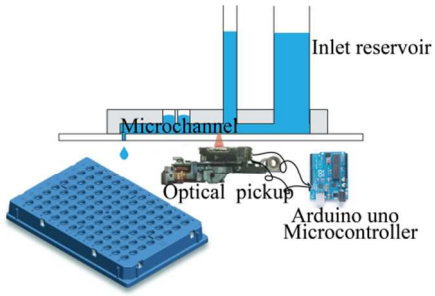

Figure 1: Schematic of the experimental setup demonstrating device principle. The DVD optical pickup controlled by the Arduino microcontroller generates the optical trap that isolates single microparticles inside the microfluidic device and delivers them as free falling droplets to substrates such as 96 well-plates.

Our approach of isolating cells with an optical trap and delivering them as free falling droplets in a gravity-driven microfluidic device with no active elements requires a bridge across wide-ranging length and force scales. Functioning at the µm scale with individual cells for deposition onto well plates at the mm scale constitutes a thousand-fold leap. In addition we must apply pN-scale forces to isolate single cells in fluid while dealing with mN-scale forces (Supplementary section 2) involved in generating falling droplets in the same microfluidic device. To address this, we implement a combination of passive microfluidic elements while taking advantage of an optical trap to generate non-contact forces necessary for microparticle and cell isolation.

2.1. Microfluidic design

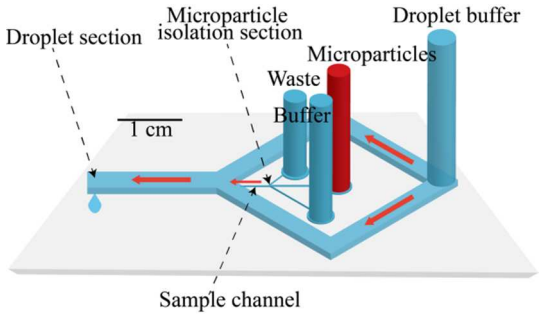

Figure 2: Schematic of the microfluidic chip identifying individual reservoirs and flow directions. Reservoir in red supplies microparticles that flow into the waste reservoir until the optical trap isolates them into the sample channel leading to the droplet delivery section. Channels in the isolation section are 10 µm tall, the droplet buffer channels are 160 µm high and 3 mm wide, while channel lengths are according to scale. (Red arrows indicate flow direction).

Our microfluidic device (Figure 2) incorporates a separate isolation region to deliver single cells to the droplet generation section for distribution as droplets, an approach that shields the particle isolation section from the mN range surface tension forces involved in droplet generation. In this, an on-chip droplet buffer reservoir generates µl s^{-1} flow rates in wide channels that bifurcate at the droplet buffer inlet and wrap around the isolation section. Cells flowing into the intersection of these bulk channels via the sample channel at the end of the isolation section are carried by these relatively large flows along the 20 mm length of this channel to the microfluidic device exit, rapidly amplifying the µm translation achieved by the optical trap to mm range. This process moves particles away from the crowded isolation section to the exit where a hydrophobic orifice aids free-falling droplet generation making them easily accessible. Complete dimensions of the device are provided in supplementary section 3.

2.1.1. Single particle isolation

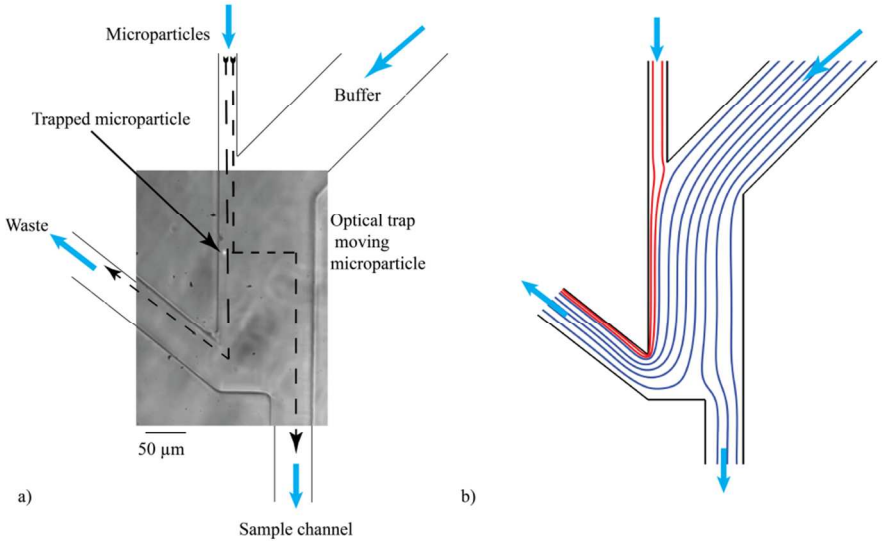

Figure 3: a) Schematic of the microparticle isolation section overlaid on actual image to demonstrate the mechanism of particle isolation. Particles flowing into this section follow streamlines into the waste channel unless translated by the optical trap into the sample channel leading into the droplet section. Channel height in this section is 10 µm and widths are according to scale. b) Comsol simulation showing streamlines and the overall flow profile.

Gravity head in the on-chip reservoirs powers the isolation section (Figure 2). The pl s^{-1} flow rates in the 100 µm by 10 µm isolation section lead to a laminar flow profile (Reynolds number, $Re = 4hV\rho/\mu \sim 10^{-4}$, where V is the flow velocity, h is the channel height, ρ is the fluid density and μ is the viscosity). In addition however, because the associated Peclet numbers ($Pe = aV/D$, where a is the radius, and D is the diffusion coefficient) are > 1000, microparticles remain within streamlines unless external forces are applied[27]. As illustrated in Figure 3b, particles that enter this section will exit into the waste channel unless the optical trap translates them across the channel into streamlines directed toward the droplet generation section.

2.2. Optical trap

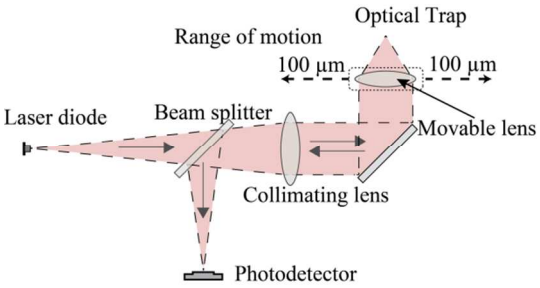

Figure 4: DVD optical pickup unit schematic demonstrating the optical components used to generate and move the optical.

To apply the pN forces needed to isolate RBCs, we employ a 200 mW, 800 nm, 3 µm x 1 µm linear diode bar laser (SDL 5432) collimated and focussed into a tight spot (150 mW at sample plane) using a pair of symmetric 20x aspheric lenses (NA ~ 0.53, Newport 5724-B-H). For the lower optical powers required for manipulating polystyrene microparticles we use an inexpensive and compact off-the-shelf DVD optical pickup unit[26]. With the added benefit of reduced cost and small footprint, this unit includes a 500 mW 660 nm laser diode that is focused into a 2 µm spot (70 mW at sample plane due to losses in the optical path) using the integrated optics (NA ~ 0.6) (Figure 4) to generate up to 15 pN of optical trapping force[26]. We also employ the electromagnetically suspended movable focusing lens of the optical pickup unit driven by an inexpensive programmable microcontroller (Arduino UNO). This is used to translate trapped particles across the microfluidic channel into the sample exit channel. A separate photoresistor (GL55 Series, Senba Optical & Electronic Co./ LTD.) was placed in the sample plane at ~90° to the optical path to measure laser sidescatter from trapped particles.

2.3. Hydrofocusing stripes

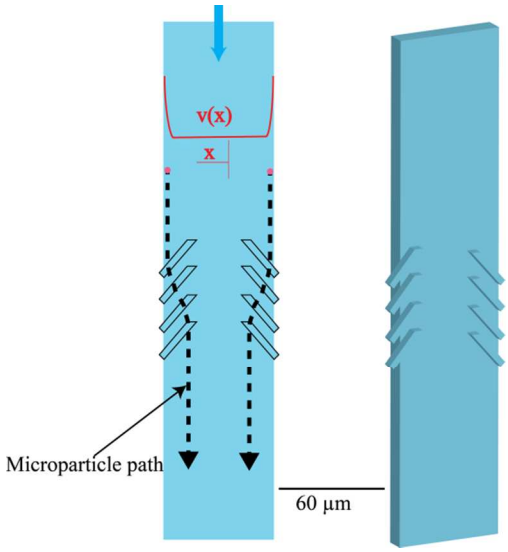

Figure 5: Schematic of the stripe location and function along with perspective view of the sample channel. The black dotted line illustrates the cell or microparticle path as they are moved away from the wall by the stripes. Velocity profile across the centre of the channel, from Comsol simulation, is plotted in red.

In the low channel aspect ratio sample channel (height/width = 0.25) the flow velocity is low close to the edge but increases rapidly away from the side walls[28] (red velocity profile in Figure 5). To prevent particles from remaining too long in this region, we implement stripes developed by Howell *et al.*[29] in a herringbone pattern (Figure 5) to passively focus particles ~10 µm into the center region with faster flow velocities. These 20 µm wide and 10 µm deep stripes in the microfluidic channel roof are inclined 45° to flow and reduce particle residence times to ~15 s in this section. In addition, flow velocities away from the wall are more uniform making arrival times at the end of this section readily predictable.

2.4. Droplet generation section

Microparticles drain into the droplet generation section from the sample channel and are carried to the exit. Here, 750 µm holes were drilled through a glass substrate and the underside of the device was made hydrophobic by treating it with Rainx® windshield hydrophobic treatment (Illinois ToolWorks, Inc.). At this exit the fluid forms droplets that fall, as surface tension can no longer hold them. This simple device was tested by dispensing droplets of 0.5% sodium dodecyl sulphate (SDS) in DI water solution from a gravity-driven micro-channel at a rate of 2 s^{-1} with a measured tight weight distribution of 53.72 ± 0.07 mg. We have observed consistent and predictable droplet generation frequency over 500 samples collected over 10 hours of continuous operation demonstrating potential for generation of large number of samples in a single experiment. By mapping particle residence times with the predictability of droplet formation timing, we can time isolated particles for arrival at the drain at the early stage of the droplet formation cycle for encapsulation within a specific droplet.

2.5. Backpressure

Falling droplets create significant backpressures due to the sudden change of interfacial area at the exit air/water interface. These oscillations have mN amplitudes (See Supplemental section 2 for derivation), very strong compared to the optical trap strength of 15 pN, inhibiting proper particle isolation scheme function if not properly shielded. We address this by both designing appropriate resistances and with the incorporation of compliance reservoirs. For resistances, channels in the isolation section are much smaller compared to the droplet generation section increasing their fluidic resistance,

$$R \approx \frac{12\mu L}{wh^3} \qquad (1)$$

where μ is the viscosity, L is the length of the channel, w is the width of the channel and h is the channel height[30]. As a result, the resistance of the thin and narrow isolation section channels is 10^5 times that of the tall and wide channels in the droplet generation section. Therefore backpressure waves predominantly take the low resistance path, avoiding the isolation section.

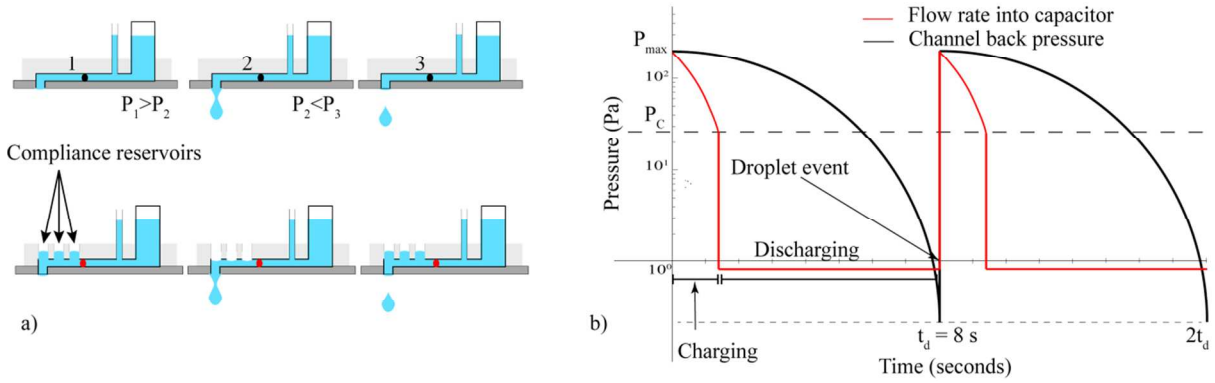

Figure 6: a) Operating principle of the hydrophobic compliance reservoirs. P_1, P_2 and P_3 are the pressures at the channel locations marked by the black dot. As the droplet forms, pressure upstream of the channel falls until spikes are induced by droplet falling. These spikes are dampened by the compliance reservoirs before they travel upstream. b) Representative plots of the pressure oscillations in the channel and the observed fluidic capacitor charging and discharging curve vs. channel back pressure. P_{max} is the maximum pressure in the channel near the compliance reservoirs and P_C is the compliance reservoir capillary pressure.

2.5.1. Compliance reservoirs

To further dampen oscillations, compliance reservoirs[31] ~2 mm diameter hydrophobic reservoirs were added downstream of the particle isolation section to absorb pressure waves from falling droplets (Figure 6a) and designed to dampen the high amplitude oscillations. These minimize the spike in local pressure with slow discharge while the next droplet forms, preventing large pressure waves from moving upstream and affecting microparticle isolation.

Droplet backpressure can be described as a sawtooth oscillation while the compliance reservoirs act as bypass capacitors when considered in the electrical circuit analogy. Here, compliance reservoirs behave as infinite capacitors at a constant pressure P_C, the capillary pressure, unlike the more commonly used charge dependent membrane capacitors[32] whose pressure scales with accumulated volume. These are charged infinitesimally when the bulk channel pressure is greater than P_C and discharge when the bulk channel pressure is less than P_C. P_C is at the interface in the cylindrical compliance reservoirs and is $2\sigma Cos\theta/r$, where r is compliance reservoir radius, θ is the contact angle of water/air/PDMS and σ is the surface tension at the air/water interface. To determine the size of the compliance reservoir required we apply a circuit analysis (Figure 7) with P_S the sorting section pressure head, P_D the droplet buffer pressure head, P_C the constant pressure on the capacitor, and P_B the oscillatory backpressure due to falling droplets. Fluidic resistances estimated using Eq. 1 include the bulk section resistances R_{B1} and R_{B2}, the sort section resistance R_S and the small resistance of channel between compliance reservoirs and exit R_E. C_C is the volume of compliance reservoirs and is very large compared to back flow volumes. P_C must be greater than the local pressure to prevent flow leaking into the compliance reservoir except when there is a pressure increase. R_E is designed to be significantly smaller than R_{B1} and R_{B2} to prevent back flow in the channel when the capacitor discharges. The rate of charging of the capacitor is proportional to $(P_B - P_C)$ for constant R_E. The rate of discharging of the capacitor is proportional to P_C and can be used to smooth the pressure oscillation by temporally spreading feedback. The estimated capacitor charging and discharging behavior is illustrated in Figure 6b in relation to the backpressure to demonstrate this smoothing functionality.

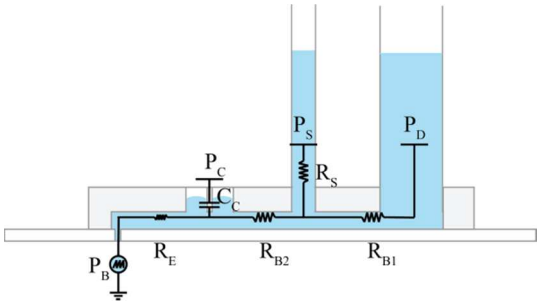

Figure 7: Device electrical circuit equivalent. Gravity heads create a constant pressure source, channels provide hydrodynamic resistance, compliance reservoirs act as fluidic capacitors and droplet backpressure creates a periodic sawtooth oscillatory pressure source (circuit analysis details are given in Supplemental section 3).

2.6. Materials

Devices were fabricated in polydimethylsiloxane (PDMS) (Sylgard 184, Dow Corning) on glass slides using standard soft-lithography techniques[33]. In this, chrome plated glass masks were printed and used to selectively polymerize KMPR 1010 and

1050 photoresist (Kayaku Microchem) via UV exposure in a mask aligner (Karl Suss MJB3) on a silicon wafer to form the masters. These templates were then used to mold PDMS that was subsequently irreversibly bonded to glass slides using oxygen plasma. The microparticles used in the experiments were surfactant-free Dragon green fluorescent plain polystyrene (FS05F/10536 Bangs Laboratories, Inc) with a mean diameter of 4.18 μm. Sample solutions were prepared in 0.25 μm filtered DI water using 2% sodium dodecyl sulfate (SDS) as surfactant. Fluorescent particles in the generated samples were counted using an epifluoresence microscope (Olympus IX81F-3). For RBC experiments, 5 μl blood collected via finger prick from anonymous donors was diluted in 1 ml of 300 mOsm phosphate buffered saline with 1.5% sodium citrate to prevent coagulation and 0.2% w/v BSA as surfactant. These cells were then fixed with 0.005% w/v glutaraldehyde, delivered to the microlfuidic device to generate single cell containing droplets imaged with a confocal microscope (Olympus FluoView FV10i) to count number of cells. For polystyrene microparticle experiments buffer, microparticle, waste and droplet buffer reservoirs were set at 7.5 cm, 4.5 cm, 2.5 cm and 7 cm gravity heads respectively. Fluid level in the droplet buffer reservoir was held constant with a siphon mated to a large external reservoir. This arrangement decouples flow disturbances caused by connector tubing while providing finer control on the fluid height. This also facilitates handling flow rates of up to 300 μl min^{-1} while keeping the chip simple by avoiding the need for sealed connectors. To characterize the flow amplification and droplet generation sections, we implemented a standard imaging system using a 20x/.45 Zeiss achroplan objective coupled to a Silicon Video high-speed SV9M001 camera. We employed an automated stage to move a cover slide or well plate into position to collect exactly one droplet before translating to the next collection point demonstrating automated delivery of multiple samples.

3. Results & Discussion

3.1. Compact prototype device characterization

To quantify the efficiency of the compact prototype device, we have isolated fluorescently tagged 4.18 μm polystyrene particles where samples dispensed as droplets were collected on cover slips to facilitate post-delivery characterization of single fluorescent particles. Particle isolation was triggered by the user after particle capture detection using a combination of sidescatter signal and bright field microscopy while particle fluorescence was used only for post-delivery quantification of dried samples. We compare the distribution of the number of particles per sample to a Poisson distribution $P(x)$, expected for stochastic delivery at equivalent bulk sample concentrations (Figure 8). For a droplet having exactly x particles, $P(x) = e^{-\lambda}(\lambda^x/x!)$ where λ is the average number of particles per droplet volume in the bulk sample[34]. With 200 samples generated at a particle delivery rate of 100 hr^{-1}, we achieved 78% single-particle sample droplet accuracy, twice of what is expected for a bulk stochastic process. In addition, only 8% of samples generated were blanks occurring if particles stuck to the channel walls or if the droplet was collected before or after the particle arrived at the exit. 14% of samples were doublets and were primarily due to the optical trap isolating two particles at a time. To identify such isolation errors, we employed a basic sidescatter based detection scheme along with bright-field microscopy, an approach necessary as there is a statistical probability that two particles will end up within the trap due to its finite residence time in flow. To predict this natural frequency, we define the normalized particle concentration $\varphi = C\upsilon\tau wh$ where C is the particle concentration of the microparticle sample flowing into the isolation section, υ is average fluid flow velocity in the isolation section, τ is the time taken for detection and translation, h is the height of the microfluidic channel in the isolation section and w is the width of the trapping zone. The probability for a doublet is the probability of one more particle flowing into the optical trap before the trap can move away and is now defined via the Poisson distribution as $P_{err}(\varphi) = \sum_1^\infty e^{-\varphi}(\varphi^x/x!) = 1 - e^{-\varphi}$. This dependence predicts least chance for doublets in a system when the average particle concentration, flow velocity and the detection time are set to the least practicable values for that particular application. For our system where C= 3x10^7 mL^{-1}, h = 10 μm, w = 10 μm, τ = 1.2 s and υ = 60 μm s^{-1}, a 20% chance of a doublet every time the optical trap attempts single-particle isolation is predicted. Our detection system identified several of these doublets (~10 % of capture events) but missed others because of their doublet orientation in the trap. An advanced detection scheme or an optical trap with trap spot size designed to trap precisely one particle would further reduce the doublets.

It is also instructive to discuss the theoretical limits of this compact prototype device where maximum throughput is governed by the highest frequency at which the optical trap can translate particles 60 μm across the microfluidic channel from the waste to the sample stream (Figure 3a). For 4.18 μm polystyrene microparticles and for our current setup this is ~ 0.5 s^{-1} using a maximum translation speed of 60 μm s^{-1} limited by viscous drag forces overcoming optical trap force. For polystyrene particles this leads to a throughput of 3600 hr^{-1} and for typical biological cells with a much smaller maximum translational speed limit (5 μm s^{-1}), this translates to ~200 hr^{-1}. While being competitive in cost with the laborious limiting dilution technique, the accuracy achieved by our proof-of-concept device motivates the development of a similar compact and efficient optical trapping module with laser wavelength, beam shape and optical power tuned to work with cells.

3.2. Red blood cell delivery efficiency

To demonstrate the ability of the microfluidic device to isolate and deliver single RBCs we employed a bench-top optical trap to deliver droplets on cover slips, which were then scanned using confocal fluorescence microscopy to identify individual cells post-delivery. Glutaraldehyde was used to both stabilize the cells over the 30 min necessary for proper characterization of each sample and provide a bright non-specific fluorescent tag for clear identification (fluorescence filter EYFP, EX: 480 nm, EM: 527 nm)[35]. Though we can consistently deliver hundreds of single cells samples in a single experiment at 100 hr^{-1}, challenges involved in the detection of a single RBC in a 50 µl droplet post-delivery limit the total number of samples characterized. It can be seen from Figure 8 that the device generated fewer doublets and a higher number of blanks while isolating red blood cells (Red is Figure 8) when compared to the microparticle system (Blue in Figure 8). This reduction in the number of doublets can be attributed to the stronger and size-matched optical trap that consistently traps only one cell at a time. We attribute the increase in blanks to the stickiness of RBCs, which tend to adhere to the channel walls more than microparticles increasing the variance of residence times and cells missing the collected droplet.

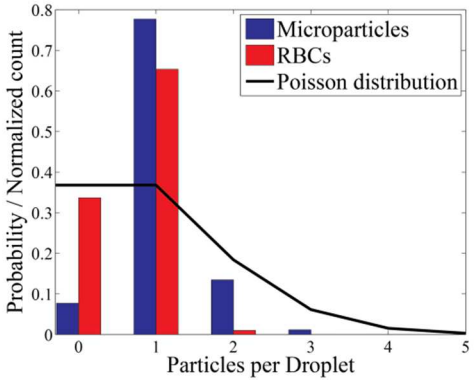

Figure 8: Sample distribution of single microparticle samples (blue) delivered by the DVD-based device based on collected droplets of 200 sorted polystyrene microparticles compared to a Poisson distribution expected from stochastic delivery (black). Also shown is the sample distribution of single RBC samples (red) isolated with the bench-top optical trap based on collected droplets of 101 sorted RBCs, analysed across 6 experiments.

4. Conclusions

We demonstrate a simple microfluidic dispenser for applications that require single microparticle/cell isolation and delivery with minimal instrumentation. The absence of active elements or moving parts apart from the optical trap leads to simplicity of operation and reduced operating cost. The device can function in a continuous mode that can be operated indefinitely for applications where a significant number of samples are required. This droplet generation concept can potentially be integrated with any microfluidic platform as a means to deliver particles or samples from the micro to the macro-world, with benefits and accuracies achievable only in a microfluidic chip.

5. Acknowledgements

We acknowledge support from the National Institutes of Health under grant 1R01 AI079347-01 and thank Kevin Roth, Allison Tyner and Maria Monroe for useful discussions.

References

1. K. Dotan, B. Feldman, B. Goldman, Y. Peri, and L. Peleg, *J. Assist. Reprod. Genet.*, 2010, **27**, 335–341.

2. S. Ishii, K. Tago, and K. Senoo, *Appl. Microbiol. Biotechnol.*, 2010, **86**, 1281–1292.

3. K. Alain and J. Querellou, *Extremophiles*, 2009, **13**, 583–594.

4. F. Schut, E. J. de Vries, W. Harder, R. A. Prins, and D. K. Button, *Appl. Environ. Microbiol.*, 1993, **59**, 2150–2160.

5. B. F. Brehm-Stecher and E. A. Johnson, *Microbiol. Mol. Biol. Rev.*, 2004, **68**, 538–559.

6. A. Y. Fu, C. Spence, A. Scherer, F. H. Arnold, and S. R. Quake, *Nat. Biotechnol.*, 1999, **17**, 1109–1111.

7. P. H. Bessette, X. Hu, H. T. Soh, and P. S. Daugherty, *Anal. Chem.*, 2007, **79**, 2174–2178.

8. J. D. Adams, U. Kim, and H. T. Soh, *Proc. Natl. Acad. Sci. U S A*, 2008, **105**, 18165–18170.

9. A. J. Link, K. J. Jeong, and G. Georgiou, *Nat. Rev. Microbiol.*, 2007, **5**, 680–688.

10. U. Kim, J. Qian, S. A. Kenrick, P. S. Daugherty, and H. T. Soh, *Anal. Chem.*, 2008, **80**, 8656–8661.

11. J. An, J. Lee, S. H. Lee, J. Park, and B. Kim, *Anal. Bioanal. Chem.*, 2009, **394**, 801–809.

12. K. L. Chan, N. G. Green, M. P. Hughes, and F. Morgan, IEEE, 1998, vol. 6, pp. 2953–2956.

13. C. Simonnet and A. Groisman, *Anal. Chem.*, 2006, **78**, 5653–5663.

14. M. A. McClain, C. T. Culbertson, and S. C. Jacobson, *Anal. Chem.*, 2001, **73**, 5334–5338.

15. B. Yao, G.-A. Luo, X. Feng, W. Wang, L.-X. Chen, and Y.-M. Wang, *Lab Chip*, 2004, **4**, 603–607.

16. U. Kim and H. T. Soh, *Lab Chip*, 2009, **9**, 2313–2318.

17. A.-E. Saliba, L. Saias, E. Psychari, N. Minc, D. Simon, F.-C. Bidard, C. Mathiot, J.-Y. Pierga, V. Fraisier, J. Salamero, V. Saada, F. Farace, P. Vielh, L. Malaquin, and J.-L. Viovy, *Proc. Natl. Acad. Sci. U S A*, 2010, **107**, 14524–14529.

18. R. W. Applegate, J. Squier, T. Vestad, J. Oakey, and D. W. M. Marr, IEEE, 2005, vol. 3, pp. 2299–2301.

19. M. P. MacDonald, G. C. Spalding, and K. Dholakia, *Nature*, 2003, **426**, 421–424.

20. T. D. Perroud, J. N. Kaiser, J. C. Sy, T. W. Lane, C. S. Branda, A. K. Singh, and K. D. Patel, *Anal. Chem.*, 2008, **80**, 6365–6372.

21. X. Wang, S. Chen, M. Kong, Z. Wang, K. D. Costa, R. A. Li, and D. Sun, *Lab Chip*, 2011, **11**, 3656–3662.

22. L. Chen, A. Manz, and P. J. R. Day, *Lab Chip*, 2007, **7**, 1413–1423.

23. C. L. Hou and A. E. Herr, *Analyst*, 2013, **138**, 158–163.

24. O. Gutmann, R. Kuehlewein, S. Reinbold, R. Niekrawietz, C. P. Steinert, B. de Heij, R. Zengerle, and M. Daub, *Lab Chip*, 2005, **5**, 675–681.

25. E. Primiceri, M. S. Chiriaco, R. Rinaldi, and G. Maruccio, *Lab Chip*, 2013, **13**, 3789–3802.

26. A. Kasukurti, M. Potcoava, S. A. Desai, C. Eggleton, and D. W. M. Marr, *Opt. Express, OE*, 2011, **19**, 10377–10386.

27. J. Oakey, J. Allely, and D. W. M. Marr, *Biotechnol. Prog.*, 2002, **18**, 1439–1442.

28. J. P. Brody, P. Yager, R. E. Goldstein, and R. H. Austin, *BPJ*, 1996, **71**, 3430–3441.

29. P. B. Howell, D. R. Mott, F. S. Ligler, J. P. Golden, C. R. Kaplan, and E. S. Oran, *J. Micromech. Microeng.*, 2008, **18**.

30. D. J. Beebe, G. A. Mensing, and G. M. Walker, *Annu. Rev. Biomed. Eng.*, 2002, **4**, 261–286.

31. Y. J. Kang and S. Yang, *Lab Chip*, 2012, **12**, 1881.

32. D. C. Leslie, C. J. Easley, E. Seker, J. M. Karlinsey, M. Utz, M. R. Begley, and J. P. Landers, *Nat. Phys.*, 2009, **5**, 231–235.

33. D. C. Duffy, J. C. McDonald, O. J. A. Schueller, and G. M. Whitesides, *Anal. Chem.*, 1998, **70**, 4974–4984.

34. L. Mazutis, J. Gilbert, W. L. Ung, D. A. Weitz, A. D. Griffiths, and J. A. Heyman, *Nat. Protoc.*, 2013, **8**, 870–891.

35. J. S. Collins and T. H. Goldsmith, *J. Histochem. Cytochem.*, 1981, **29**, 411–414.